LA-UR-74-880

CONF-740646--1

TITLE: POTENTIAL-ENERGY SURFACES FOR HEAVY-ION COLLISIONS

AUTHOR(S): J.R. NIX
A.J. SIERK

SUBMITTED TO: NOBEL SYMPOSIUM ON SUPERHEAVY ELEMENTS, JUNE 10-15, 1974 RONNEBY, SWEDEN

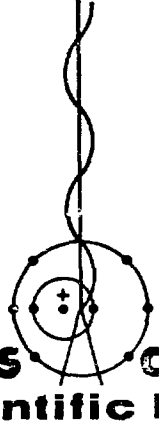

los alamos
scientific laboratory
of the University of California
LOS ALAMOS, NEW MEXICO 87544

Form No. 836
St. No. 2629
1/73

UNITED STATES
ATOMIC ENERGY COMMISSION
CONTRACT W-7405-ENG. 36

Potential-Energy Surfaces for Heavy-Ion Collisions[1]

J. R. Nix and A. J. Sierk

Los Alamos Scientific Laboratory, University of California, Los Alamos, New Mexico, U. S. A.

June 1, 1974

Heavy-particle-induced reactions and scattering

Abstract

Potential-energy surfaces for heavy-ion collisions. J. R. Nix and A. J. Sierk (Los Alamos Scientific Laboratory, Los Alamos, New Mexico, U.S.A.). Physica Scripta (Sweden).

We calculate the nuclear potential energy of deformation for the collision of two heavy nuclei by means of a macroscopic-microscopic method. The nuclear macroscopic energy is calculated in terms of a double volume integral of a Yukawa function, and the microscopic shell and pairing corrections are calculated by use of Strutinsky's method from the single-particle levels of a realistic diffuse-surface single-particle potential. The time evolution of the system after the point of first contact is determined by solving the classical equations of motion for incompressible, irrotational hydrodynamical flow. The effect of nuclear viscosity on the fusion path is to slow down the formation of the neck and to inhibit the excitation of collective shape vibrations. For nuclear systems in which

---

[1]This work was supported by the U. S. Atomic Energy Commission.

the fission saddle point lies well outside the contact point it is possible to interpret experimental fusion cross sections at relatively low bombarding energies in terms of a one-dimensional interaction barrier, as is customarily done. For heavier nuclear systems and higher bombarding energies, where the larger Coulomb and centrifugal forces tend to deform the fusing nuclei and lead to immediate fission, only those dynamical paths that pass inside the fission saddle point contribute significantly to fusion.

1. Introduction

Thus far in this symposium we have been concerned primarily with the nuclear potential energy of deformation in connection with fission, shape isomeric states, and nuclear ground-state masses and deformations. We would like now to turn to the potential energy for the collision of two heavy nuclei, which leads to different nuclear shapes and the possibility of larger nuclear systems than are encountered in these other areas. But otherwise they are all part of a common discipline associated with the shape dependence of the nuclear Hamiltonian and can be treated in a unified way.

As we have seen throughout the symposium, there are two general approaches for calculating the nuclear potential energy of deformation: selfconsistent microscopic methods and the macroscopic-microscopic method. We have learned this morning of the considerable progress that has been made recently in the former methods, and perhaps soon the potential energy

calculated this way will be sufficiently accurate to reproduce experimental observations. But our considerations here are based on the latter method [1-6]. In addition to being computationally simpler and more accurate, the decomposition of the energy into a smoothly varying macroscopic part and a fluctuating microscopic correction term permits a qualitative interpretation that is often lacking in the selfconsistent microscopic methods.

2. Macroscopic energy

The macroscopic energy is calculated frequently by means of the liquid-drop model or the droplet model [7,8], which are expansions of the nuclear energy in powers of $A^{-1/3}$ and $[(N-Z)/A]^2$. However, all such expansions break down for two nearly touching nuclei and for shapes with small necks. In these cases the finite range of the nuclear force leads to an additional reduction in energy that must be taken into account. This we do by calculating the nuclear macroscopic energy by means of a double volume integral of a Yukawa function [9], in analogy with the calculation of the Coulomb energy by means of a double volume integral of the Coulomb interaction.

To lowest order in the Yukawa range this method yields the surface energy of the liquid-drop model. For a finite Yukawa range the resulting nuclear interaction energy for two separated nuclei is similar to that calculated in other approaches [10-17]. The primary advantage of the present method is that it can be used to calculate the nuclear macroscopic energy for any conceivable shape. Its primary disadvantage is that the

effective two-nucleon interaction that is used does not contain any aspects of nuclear saturation.

To be specific, the nuclear macroscopic energy relative to the spherical shape is given by [9]

$$\Delta E_{nm} = E_{nm} - E_{nm}^{(0)} \quad , \tag{1}$$

where

$$E_{nm} = -\frac{1}{2}\left(\frac{a}{r_0}\right)^2 \frac{c_s}{4\pi^2 a^6}\int\int \frac{e^{-|\underset{\sim}{r} - \underset{\sim}{r}'|/a}}{|\underset{\sim}{r} - \underset{\sim}{r}'|/a}\, d^3r\, d^3r' \tag{2}$$

and where

$$E_{nm}^{(0)} = -\frac{2}{3}\frac{r_0}{a} c_s A + c_s A^{2/3} - \left(\frac{a}{r_0}\right)^2 c_s + \left(A^{1/3} + \frac{a}{r_0}\right)^2 c_s e^{-2\frac{r_0}{a}A^{1/3}} \tag{3}$$

is the value of E_{nm} for a sphere. The integration in eq. (2) is over the volume of the shape, whose magnitude is held fixed at $\frac{4\pi}{3} r_0^3 A$ as the nucleus deforms.

For small deformations an expansion of E_{nm} in powers of $A^{-1/3}$ leads to an A^1 term that remains constant with deformation and to an $A^{2/3}$ term that is proportional to the surface area. Because the effective two-nucleon interaction that is used is nonsaturating, the magnitude of the volume-energy term is incorrect, but this term cancels when eqs. (2) and (3) are subtracted to give the energy relative to a sphere. The constant that defines the strength of the Yukawa function is chosen so that the surface energy of a spherical nucleus is $c_s A^{2/3}$; the dependence of c_s upon nuclear

composition is taken to be

$$c_s = a_s\left[1 - \kappa\left(\frac{N - Z}{A}\right)^2\right], \tag{4}$$

where a_s is the surface-energy constant and κ is the surface-asymmetry constant. The $A^{1/3}$ term, which represents the curvature energy, is identically zero, which agrees with a recent determination of the value of the curvature-energy constant from experimental fission-barrier heights [8]. The A^0 term and the exponentially small term are strong functions of deformation and contain effects associated with the finite range of the nuclear force; these terms would be zero if the Yukawa range a were zero.

The macroscopic energy calculated in this way contains four constants, whose preliminary values are

$$r_0 = 1.16 \text{ fm}, \tag{5a}$$

$$a = 1.4 \text{ fm}, \tag{5b}$$

$$a_s = 24.7 \text{ MeV}, \tag{5c}$$

and

$$\kappa = 4.0. \tag{5d}$$

The value of the equivalent sharp-surface nuclear-radius constant r_0 was taken from an analysis of electron-scattering experiments [18], and the values of the remaining constants were determined [9] from adjustments to experimental fission-barrier heights and heavy-ion interaction-barrier heights. Because we use a shape with a sharp surface, the Yukawa range a is somewhat larger than the actual nuclear-force range in order to simulate the diffuseness of

the surface. Although the individual values of a_s and κ are determined poorly, the value of the effective surface-energy constant c_s appropriate to heavy nuclei is determined more accurately. Our value for c_s is somewhat larger than the value obtained in the liquid-drop model when experimental fission-barrier heights are used in its determination [19], but is approximately equal to the value determined from nuclear ground-state masses alone [20].

The incorporation of finite-range effects into the nuclear macroscopic energy leads to several important consequences [9]. First of all, higher-multipole distortions do not increase the energy as much as in the liquid-drop model. The calculated ground-state hexadecapole moments for the lighter actinide nuclei are therefore larger [21] than those calculated with the liquid-drop model. For light nuclei, where the range of the nuclear force becomes a substantial fraction of the nuclear radius, the stiffness with respect to low-multipole distortions is also reduced. This lowers the fission barriers of nuclei near silver by about 10 MeV relative to those calculated with the liquid-drop model and shifts the critical Businaro-Gallone point (where stability against mass asymmetry is lost) from $Z^2/A = 19.6$ to $Z^2/A = 23.0$. For ^{40}Ca and certain other light nuclei the reduced stiffness also makes it possible for single-particle effects to create a secondary minimum in the potential energy as a function of deformation. Finally, the effective nuclear-radius parameter that frequently is used to characterize experimental interaction-barrier heights decreases for heavier nuclear systems because of the increase in the relative importance of the Coulomb interaction energy compared to the nuclear interaction energy. Each of these predicted effects is supported by some experimental data.

3. Potential-energy surfaces

An example of the potential energy calculated in this way is shown in Fig. 1 for the head-on collision of two spherical ^{84}Kr nuclei. The potential energy is plotted as a function of the distance r between the centers of mass of the two halves of the system, for a specified one-dimensional sequence of shapes. These shapes are generated by assuming that after the nuclei come into contact the nuclear density remains constant throughout the shape and that the displaced matter simply fills in the neck region. The shape of the neck is described by a quadratic surface of revolution that joins smoothly with the two end nuclei [22], which are assumed to remain spherical with constant radii. The limiting shape generated in this way is a slightly prolate spheroid, and pure spheroids are used to describe the shapes to the left of this point.

Our potential-energy surfaces apply only when the relative velocities after contact are small compared to the nuclear sound speed, for which the assumption of constant nuclear density should be approximately valid. At higher incident energies, the increase in density in the neck region [23-25] would lead to an increase in potential energy as the nuclei come together [10, 17, 25, 26]. At still higher energies, other phenomena such as meson and baryon production, nuclear hot spots, and nuclear vaporization should also become important [24].

When the angular momentum is nonzero, there is an additional effective repulsive potential, as illustrated in Fig. 2. The discontinuities in the curves arise from the assumption that after the two nuclei come into contact the system begins to rotate as a rigid body. (The system is assumed to

remain axially symmetric about a line that rotates in space.) This increases the moment of inertia from μr^2 prior to contact to $\mu r^2 + I_1 + I_2$ after contact, where μ is the reduced mass and I_1 and I_2 are the rigid-body moments of inertia of the two halves of the system for rotation about their centers of mass [15, 16, 27-30].

When the target and projectile are equal spheres, the moment of inertia immediately after contact is $\frac{7}{5}$ its value immediately before contact, which reduces the total rotational energy after contact to $\frac{5}{7}$ its value before contact. This $\frac{5}{7}$ decomposes further into $\frac{25}{49}$ associated with orbital angular momentum plus $\frac{10}{49}$ associated with the spin of the two halves about their centers of mass. The remaining $\frac{2}{7}$ of the original rotational energy is dissipated into internal single-particle excitations through viscous forces. These forces are idealized here as infinitely strong, which leads to the abrupt transitions shown in Fig. 2. In an actual nucleus, the forces are of course weaker and the reduction in energy takes place over a small finite region of deformation [28, 29].

In Fig. 2 we are showing the effective potential energy corresponding to the total angular momentum because the systems's equilibrium configurations are given in terms of this quantity [31, 32]. However, for determining the system's stability against center-of-mass separation r near the contact point, the effective potential energy corresponding to the orbital angular momentum is more relevant [28, 29]. The reduction in orbital angular momentum by viscous forces can convert such an effective potential that is initially repulsive into one that is attractive.

Therefore, even at the level in which we are considering only one-dimensional interaction barriers, the determination of the fusion cross section must involve at least two considerations: First, only those angular-momentum states for which the total effective potential prior to contact lies below the center-of-mass bombarding energy will lead to fusion with appreciable probability. The critical distance at which the system becomes committed to fusion [33-36] shifts from outside the contact point for the lower states of angular momentum to the contact point itself for the higher states. (In practice this point lies somewhat inside the contact point because of the gradual rather than instantaneous reduction in rotational energy.) Second, after contact the effective potential corresponding to the orbital angular momentum must be attractive in order for fusion to occur. However, it should be noted that the point at which the system begins to rotate as a rigid body is roughly the same point at which the neck is sufficiently large to permit the transfer of mass from one nucleus to the other. Mass transfer can of course take place even though after contact the effective potential corresponding to the orbital angular momentum is repulsive.

Existing experimental fusion cross sections are described approximately in terms of the first consideration alone [33-36]. But these data cover a fairly limited region of bombarding energy and nuclear systems. At higher bombarding energies, where higher angular-momentum states are accessible, the second consideration should reduce the fusion cross section somewhat relative to that calculated from the first consideration. For heavier nuclear systems, the possibility of additional deformations (to be considered later) should reduce the fusion cross section even further.

Although most of our studies here are restricted to the macroscopic part of the energy, we have also calculated the microscopic shell and pairing corrections for the fusion of a few selected nuclei. These corrections are calculated by use of Strutinsky's method [1-6] from the single-particle levels of a realistic diffuse-surface single-particle potential of the folded Yukawa type [2-4]. As illustrated in Fig. 3, when the proton and/or neutron numbers of the colliding nuclei are near closed shells, the potential energy near the contact point is reduced substantially by single-particle effects. The distance required for a reversal of single-particle effects is much larger near the contact point than near the ground state. For two ^{136}Xe nuclei the potential energy contains a local minimum inside the contact point as a function of this one-dimensional sequence of shapes. However, this minimum is probably unstable against elongation of the two halves of the system, which would prevent the existence of a nuclear molecule. But such nuclear molecules possibly exist for lighter nuclear systems. We plan to explore these points in the near future.

As we proceed from light nuclear systems to heavy ones, there are several qualitative changes in the potential energy, as illustrated in Fig. 4. Because the repulsive Coulomb force grows faster than the attractive nuclear force, the nuclear surfaces must be brought closer together in heavier systems before the nuclear force overcomes the Coulomb force. This increases the height of the interaction barrier at a faster rate than when it is calculated by use of a constant effective nuclear-radius parameter. It also moves the maximum in the interaction barrier to smaller distances (when measured in units of the radius R_0 of the spherical final nucleus). For

very heavy nuclear systems there is no maximum at all in the interaction barrier near the contact point--the energy simply continues to increase until the sphere is reached. The local oblate minimum that occurs for these cases is unstable against axially asymmetric (gamma) deformations.

In the case of two ^{150}Nd nuclei, the energy is relatively flat between the contact point and the sphere as a function of this one-dimensional sequence of shapes. However, we should not jump to the conclusion that if these nuclei are brought together at an energy slightly above that of the contact point they will fuse to form the superheavy nucleus ^{300}120. As we see in Fig. 5, the path between the contact point and the sphere is actually on the side of a steep hill with respect to the elongation of the two halves of the system. The fragment-elongation coordinate σ shown in the figure is defined as the sum of the root-mean-square extensions along the symmetry axis of the mass of each half about its center of mass.

The use of the two central moments r and σ as generalized deformation coordinates provides a convenient way of projecting out of the multidimensional potential-energy surface the two most important symmetric degrees of freedom [4, 37, 38]. Near the sphere r and σ are related by an orthogonal transformation to the coefficients α_2 and α_4 in an expansion of the radius vector in Legendre polynomials, and for two equal separated spheroidal nuclei r is simply the distance between their mass centers and σ is proportional to their major semiaxis. (The generalization of these moments to asymmetric shapes presents the classic problem of where to divide the two portions of the system, which we are investigating but have not solved.)

For describing the variety of possible shapes in fission, different parametrizations are better suited for different regions of deformation. For most regions we have used the three-quadratic-surface parametrization [22], eliminating one of its three symmetric coordinates in some way. In particular, shapes corresponding to the liquid-drop-model saddle points and most-probable dynamical paths for values of the fissility parameter x between 0 and 1 are used in the region that is accessible in this way. Inside the spiral defined by the liquid-drop-model saddle points, the shapes are determined by holding fixed the ends of the shapes along the right-hand portion of the spiral and filling in the neck region as the ends are brought together. Shapes below this region are determined in an analogous way by starting with two tangent oblate spheroids. Two equal separated spheroids are used to describe postscission (or precontact) shapes in the binary valley. In the region above the most-probable liquid-drop-model dynamical path we use shapes described by a pure spheroid and by a cylinder with spherical ends. The latter sequence of shapes passes between the ternary and quaternary valleys, which are not accessible in the parametrization of three smoothly joined portions of quadratic surfaces. Postscission shapes in these valleys are described by, respectively, three and four equal separated spheroids. Finally, positive hexadecapole (diamond-like) shapes are described by the two coordinates ε and ε_4 in Nilsson's perturbed-spheroid parametrization [1].

The potential-energy surface as a function of r and σ depends strongly upon the nuclear system. For systems heavier than $^{300}120$ the energy decreases even more rapidly in the directions of the ternary and quaternary valleys than in Fig. 5. Although a consideration of dynamics is necessary to decide

the outcome, fission into three or four (or even more) fragments should predominate over binary fission for sufficiently heavy systems [39]. As we proceed from $^{300}120$ to lighter nuclear systems the saddle point moves from the vicinity of the sphere to locations that ultimately lie well outside the contact point. The transition from saddle points that lie inside the contact point to those that lie outside occurs roughly for the fusion of two ^{110}Pd nuclei, which forms the final nucleus ^{220}U. For nuclear systems lighter than this the forces near the contact point are directed toward the sphere, whereas for heavier systems the forces are directed toward the fission valley.

4. Dynamics

Although potential-energy surfaces are useful for many purposes, the dynamics of nuclear motion must also be considered in order to determine the time evolution of the system. This we do by solving the classical equations of motion for incompressible, irrotational hydrodynamical flow. Nuclear viscosity (the transfer of energy of collective motion into internal single-particle excitations) is introduced by means of Rayleigh's dissipation function [3, 40]. For a given set of initial conditions, Hamilton's modified equations of motion are solved numerically for the time evolution of the six coordinates and six conjugate momenta that appear in the three-quadratic-surface parametrization[22].

What is our rationale for treating nuclear dynamics in this way? First of all, the de Broglie wavelength for motion in a given direction is small compared to the distance over which the potential changes appreciably so

long as the kinetic energy in that direction exceeds about 1 MeV. Therefore, except for barrier penetration or for motion very close to the barrier, classical mechanics can be used for describing at least the motion along the fission or fusion directions. Of course, quantal zero-point vibrations lead to a distribution of values of the coordinates and momenta in the transverse directions that must be taken into account in some way.

As far as incompressibility is concerned, we noted earlier that the nuclear matter should be approximately incompressible when the relative velocities after contact are small compared to the nuclear sound speed, but it will become compressed at higher incident energies.

It is well known that nuclear flow is not irrotational for ground-state vibrational motion and for the adiabatic penetration of the fission barrier in spontaneous fission [1, 3, 5, 6]. However, at larger distortions the single-particle levels do not vary as rapidly with deformation, and at higher internal excitations the energy denominators in the cranking formula for the inertia [3, 5, 6, 41] are no longer all of one sign. Both of these effects reduce the size of the calculated inertias, and for these cases the assumption of irrotational flow should be somewhat better. Provided that the flow is initially irrotational it will remain irrotational as a function of time even in the presence of viscosity. (An important case for which this does not apply is a heavy-ion collision with angular momentum, where some curl is generated upon impact.) As an approximation to irrotational flow we use the Werner-Wheeler method, which determines the flow in terms of circular layers of fluid [22].

The coupling between the collective and internal degrees of freedom is of course also a function of the single-particle structure, but at least for large

distortions and moderate excitation energies it should be possible to treat this coupling approximately in terms of an average coefficient of nuclear viscosity.

For nonviscous nuclei in the liquid-drop model such dynamical calculations were performed several years ago for fission [22, 42] and more recently for the fusion of two nuclei [38]. Up to now the effect of nuclear viscosity on the dynamical path has been studied only for the postscission motion of spheroidal fission fragments [38], although for small values of viscosity the energy dissipated along the nonviscous path from saddle to scission has also been calculated [43]. We have now carried out calculations that include viscosity and also the finite range of the nuclear force in both fission and fusion.

For fissioning nuclei the finite range of the nuclear force increases somewhat the rate at which the neck is formed, which leads to a somewhat more constricted scission configuration and consequently a larger final fission-fragment kinetic energy than in the liquid-drop model. The calculated kinetic energy is increased even more because the nuclear radius constant that we are now using [see eq. (5a)] is 5% smaller than the value used in previous calculations [19, 22].

The effect of viscosity on the fission path is to decrease the rate at which the neck forms, which leads to a more elongated scission configuration and consequently to a smaller final fission-fragment kinetic energy. Loosely speaking, viscosity causes the system to deviate from its nonviscous path

so as to lessen the energy dissipation. The large gradients in the hydrodynamical flow pattern during neck formation lead to a large dissipation for this mode, which is therefore hindered.

Although it is impossible to speak precisely about valleys in multidimensional potential-energy surfaces, it is hard to resist imagining a fission valley in a contour diagram such as Fig. 5. The calculated most probable fission path for zero viscosity lies somewhat above this valley, and the effect of viscosity is to displace the path even farther above the valley. This presents a new difficulty for the so-called statistical theory of fission [44], which is founded on the idea that a viscous system would follow the bottom of the valley on its slow descent from saddle to scission.

From a preliminary comparison of the experimental most-probable fission-fragment kinetic energy for ^{236}U with values calculated as a function of viscosity, we estimate that the value of the coefficient of nuclear viscosity is approximately 0.01 TP. (Note that 1 TP = 1 terapoise = 10^{12} poise = 10^{12} dyne sec/cm^2.) For idealized heavy nuclei this value is roughly 0.1 times the value that is required to critically damp quadrupole oscillations. The value determined for the viscosity coefficient is unfortunately sensitive to certain details, such as the value used for the nuclear-radius constant, the possibility that the neck may rupture before its radius goes to zero, the method that is used for treating postscission motion, and the effect of single particles on the experimental kinetic energies. Until these points are resolved and nuclei throughout the periodic table are considered, the value 0.01 TP should be regarded as preliminary, even though it agrees

approximately with other recent estimates [43].

In the collision of two nuclei the dynamical path depends strongly upon the location of the fission saddle point relative to the contact point. For nuclear systems in which the saddle point lies well outside the contact point, the path proceeds in the general direction of the sphere once it has passed the maximum in the interaction barrier. However, when the saddle point lies inside the contact point, the path is deflected toward the fission valley unless the incident kinetic energy is large enough to drive the system toward the sphere. This is illustrated in Fig. 6 for the collision of two ^{150}Nd nuclei, which corresponds to the potential-energy surface of Fig. 5. Even for zero nuclear viscosity at least 50 MeV of additional kinetic energy appears necessary to drive the system from the configuration of two touching spheres to a single sphere.

For two colliding nuclei the finite range of the nuclear force decreases the rate at which the neck grows and permits the development of nuclear shapes whose ends flatten even more quickly than in the liquid-drop model [38]. However, the amount of energy that goes into collective excitations is less than in the liquid-drop model, which means that less additional kinetic energy is required to bring the system to a spherical shape.

The effect of viscosity on the fusion path is to slow down the formation of the neck, which in turn slows down the flattening of the ends. Consequently, the amount of energy that goes into collective excitations is not as large as for zero viscosity, which compensates somewhat the dissipation of energy into internal excitations. It appears that nuclear viscosity is not as harmful to fusion as had been feared [45] both because its

magnitude is relatively small and because for viscous flow the dynamical path readjusts itself in order to decrease the amount of energy dissipated.

We are now attempting to calculate fusion cross sections for heavy systems based on the idea that those dynamical paths that lead inside the fission saddle point have a high probability for fusion, whereas those that lead outside have a low probability. This entails calculating both the saddle points and the dynamical paths as functions of angular momentum. As the angular momentum increases, the saddle point moves toward the sphere [32], whereas the dynamical path is pushed away. (Several of the approximations that we are using grow worse as the angular momentum increases.) The critical angular momentum at which the fusion path first passes outside the fission saddle point determines approximately the fusion cross section.

5. Summary and conclusion

We have found that the macroscopic-microscopic method that was developed in connection with fission and nuclear ground-state masses and deformations is equally useful for calculating potential-energy surfaces for heavy-ion collisions. In this case it is necessary to take into account the finite range of the nuclear force, but this can be done in a simple way by calculating the nuclear macroscopic energy in terms of a double volume integral of a Yukawa function.

Up to the point at which the nuclei come into contact the one-dimensional interaction barriers calculated in this way are similar to those calculated

by other methods. These barriers are useful for understanding experimental fusion cross sections at relatively low bombarding energies for systems in which the fission saddle point lies well outside the contact point. However, predictions based on these barriers are expected to break down at higher bombarding energies and for heavier nuclear systems, where the deformations of the fusing nuclei become important. In these cases a promising method for calculating fusion cross sections is to determine the critical angular momentum above which the dynamical path in a multidimensional space ceases to pass inside the fission saddle point.

Acknowledgements

We are grateful to K. T. R. Davies · his collaboration on the incorporation of nuclear viscosity into the dynamical equations of motion.

References

1. Johansson, T., Nilsson, S. G. and Szymański, Z., Ann. Phys. (Paris) 5, 377 (1970).
2. Bolsterli, M., Fiset, E. O., Nix, J. R. and Norton, J. L., Phys. Rev. C 5, 1050 (1972).
3. Nix, J. R., Ann. Rev. Nucl. Sci. 22, 65 (1972).
4. Möller, P. and Nix, J. R., Proc. Third IAEA Symp. on Physics and Chemistry of Fission, Rochester, 1973, paper IAEA-SM-174/202. IAEA, Vienna, to be published.
5. Brack, M., Damgaard, J., Jensen, A. S., Pauli, H. C., Strutinsky, V. M. and Wong, C. Y., Rev. Mod. Phys. 44, 320 (1972).
6. Pauli, H. C., Phys. Rep. 7, 35 (1973).
7. Myers, W. D. and Swiatecki, W. J., Ann. Phys. (New York) 55, 395 (1969).
8. Myers, W. D. and Swiatecki, W. J., Berkeley Preprint LBL-1957 (1973).
9. Krappe, H. J. and Nix, J. R., Proc. Third IAEA Symp. on Physics and Chemistry of Fission, Rochester, 1973, paper IAEA-SM-174/12. IAEA, Vienna, to be published.
10. Scheid, W. and Greiner, W., Z. Phys. 226, 364 (1969).
11. Holm, H. and Greiner, W., Phys. Rev. Lett. 24, 404 (1970).
12. Wong, C. Y., Phys. Lett. 42B, 186 (1972).
13. Brink, D. M. and Rowley, N., Nucl. Phys. A219, 79 (1974).
14. Wilczyński, J., Nucl. Phys. A216, 386 (1973).
15. Bass, R., Phys. Lett. 47B, 139 (1973).
16. Bass, R., Frankfurt Preprint (1974).
17. Swiatecki, W. J., Physica Scripta, these Proceedings.

18. Myers, W. D., Nucl. Phys. A204, 465 (1973).

19. Myers, W. D. and Swiatecki, W. J., Arkiv Fysik 36, 343 (1967).

20. Seeger, P. A., Proc. Fourth Int. Conf. on Atomic Masses and Fundamental Constants, Teddington, 1971, p. 255. Plenum, London, 1972.

21. Möller, P., Nilsson, S. G. and Nix, J. R., Los Alamos Preprint LA-UR-74-462 (1974).

22. Nix, J. R., Nucl. Phys. A130, 241 (1969).

23. Wong, C. Y. and Welton, T. A., Phys. Lett. 49B, 243 (1974).

24. Chapline, G. F., Johnson, M. H., Teller, E. and Weiss, M. S., Phys. Rev. D 8, 4302 (1973).

25. Scheid, W., Müller, H. and Greiner, W., Phys. Rev. Lett. 32, 741 (1974).

26. Brueckner, K. A., Buchler, J. R. and Kelly, M. M., Phys. Rev. 173, 944 (1968).

27. Mosel, U., Particles and Nuclei 3, 297 (1972).

28. Swiatecki, W. J. and Tsang, C. F., unpublished (1973).

29. Tsang, C. F., Physica Scripta, these Proceedings.

30. Davis, R. H., Tallahassee Preprint (1973).

31. Lyttleton, R. A., The Stability of Rotating Liquid Masses, ch. II, pp. 6-30. Cambridge Univ. Press, Cambridge, 1953.

32. Cohen, S., Plasil, F. and Swiatecki, W. J., Ann. Phys. (New York) 82, 557 (1974).

33. Galin, J., Guerreau, D., Lefort, M. and Tarrago, X., Phys. Rev. C 9, 1018 (1974).

34. Namboodiri, M. N., Chulik, E. T., Natowitz, J. B. and Kenefick, R. A., College Station Preprint ORO-3924-17 (1974).

35. Guttrod, H. H., Winn, W. G. and Blann, M., Nucl. Phys. A213, 267 (1973).

36. Glas, D. and Mosel, U., Giessen Preprint (1974).

37. Koonin, S. E., unpublished (1972).

38. Sierk, A. J. and Nix, J. R., Proc. Third IAEA Symp. on Physics and Chemistry of Fission, Rochester, 1973, paper IAEA-SM-174/74. IAEA, Vienna, to be published.

39. Swiatecki, W. J., Proc. Second UN Int. Conf. on Peaceful Uses of Atomic Energy, Geneva, 1958, vol. 15, p. 248. UN, Geneva, 1958.

40. Goldstein, H., Classical Mechanics, ch. 1, sec. 5, pp. 19-22. Addison-Wesley, Reading, 1959.

41. Inglis, D. R., Phys. Rev. 103, 1786 (1956).

42. Hasse, R. W., Nucl. Phys. A128, 609 (1969).

43. Wieczorek, R., Hasse, R. W. and Süssmann, G., Proc. Third IAEA Symp. on Physics and Chemistry of Fission, Rochester, 1973, paper IAEA-SM-174/2. IAEA, Vienna, to be published.

44. Fong, P., Statistical Theory of Nuclear Fission. Gordon and Breach, New York, 1969.

45. Swiatecki, W. J., J. Physique Suppl. 33, Colloque C5, 45 (1972).

Figure captions

Fig. 1. Individual Coulomb and nuclear contributions and the total macroscopic potential energy for the system $^{84}Kr + {}^{84}Kr \rightarrow {}^{168}Hf$. The energies are calculated for the sequence of shapes illustrated at the bottom of the figure and are plotted as functions of the distance r between the centers of mass of the two halves of the system, in units of the radius R_0 of the spherical final nucleus ^{168}Hf. The point at which the equivalent sharp nuclear surfaces first come into contact is indicated by the dashed vertical line, and the sphere is indicated by the solid vertical line. The arrow gives the maximum in the interaction barrier.

Fig. 2. Effective macroscopic potential energies corresponding to the indicated amounts of angular momentum ℓ (in units of $\hbar$) for the system $^{84}Kr + {}^{84}Kr \rightarrow {}^{168}Hf$. The discontinuities arise from the assumption that after contact the system rotates as a rigid body.

Fig. 3. Two examples of the effect of single particles on the potential energy. The dashed curves give the macroscopic contributions, and the solid curves give the total potential energies (which have been calculated thus far only inside the contact point). The solid points indicate what the total potential energies at the contact point would be if the single-particle corrections were calculated for nuclei at infinity.

Fig. 4. Dependence of the macroscopic potential energy upon the nuclear system. For the $^{150}Nd + {}^{150}Nd \rightarrow {}^{300}120$ system the dashed curve near the sphere gives the total potential energy including single-particle effects.

Fig. 5. Potential-energy contours for $^{300}120$, in units of MeV. The separation coordinate r is the distance between the centers of mass of the two halves of the system, and the fragment-elongation coordinate σ is the sum of the root-mean-square extensions along the symmetry axis of the mass of each half about its center of mass. Single-particle corrections are included near the ground state, which would be unstable without these corrections. Dashed lines indicate that the results are affected noticably by discontinuities in the families of shapes that are used.

Fig. 6. Calculated dynamical paths for the system $^{150}Nd + ^{150}Nd \rightarrow ^{300}120$. The nuclear viscosity is zero, and the finite range of the nuclear force is taken into account in calculating the nuclear macroscopic energy. Each path corresponds to starting the system from the contact point with the indicated amount of center-of-mass kinetic energy relative to this point (in units of MeV). Because of deficiencies in the shape parametrization the dynamical calculations break down at the points indicated by the arrowheads.

Los Alamos Scientific Laboratory
University of California
Los Alamos, New Mexico 87544
U. S. A.

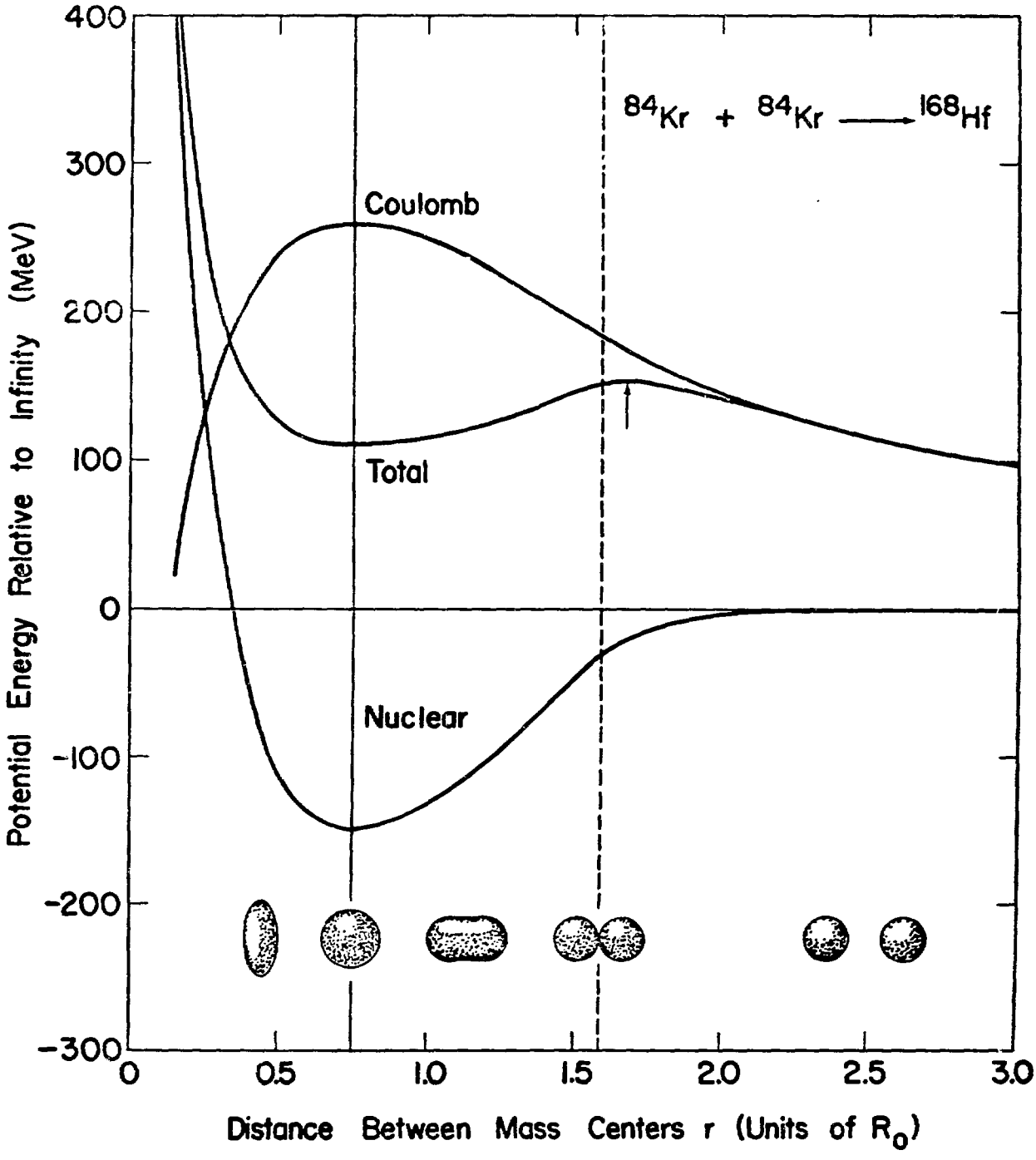
400
300
200
100
0
-100
-200
-300
0
0.5
1.0
1.5
2.0
2.5
3.0
$^{84}Kr + {}^{84}Kr \longrightarrow {}^{168}Hf$
Coulomb
Total
Nuclear
Potential Energy Relative to Infinity (MeV)
Distance Between Mass Centers r (Units of R_0)

Figure 1

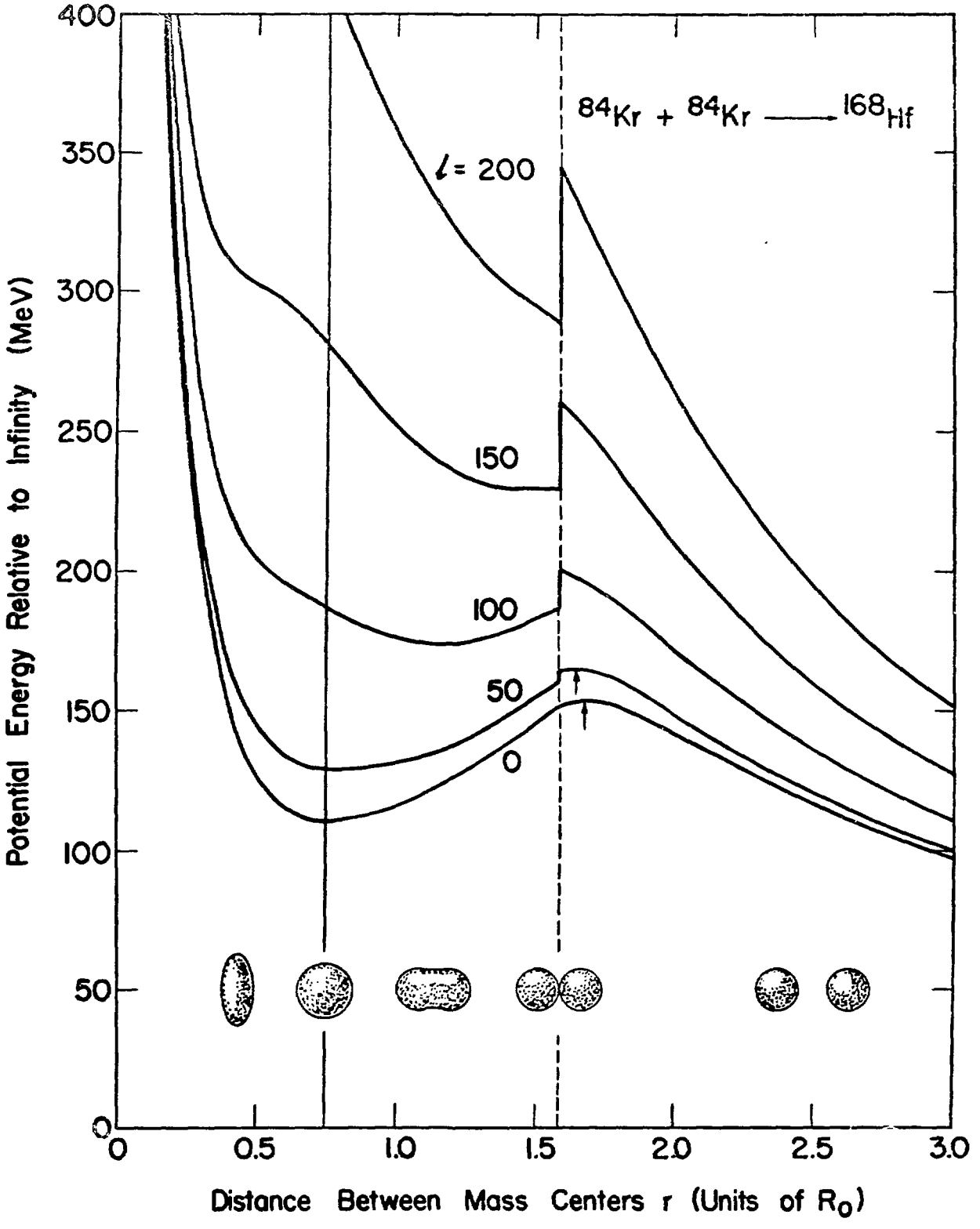
400
350
300
250
200
150
100
50
0
Potential Energy Relative to Infinity (MeV)
$^{84}Kr + ^{84}Kr \longrightarrow ^{168}Hf$
$l = 200$
150
100
50
0
0
0.5
1.0
1.5
2.0
2.5
3.0
Distance Between Mass Centers r (Units of R_0)

Figure 2

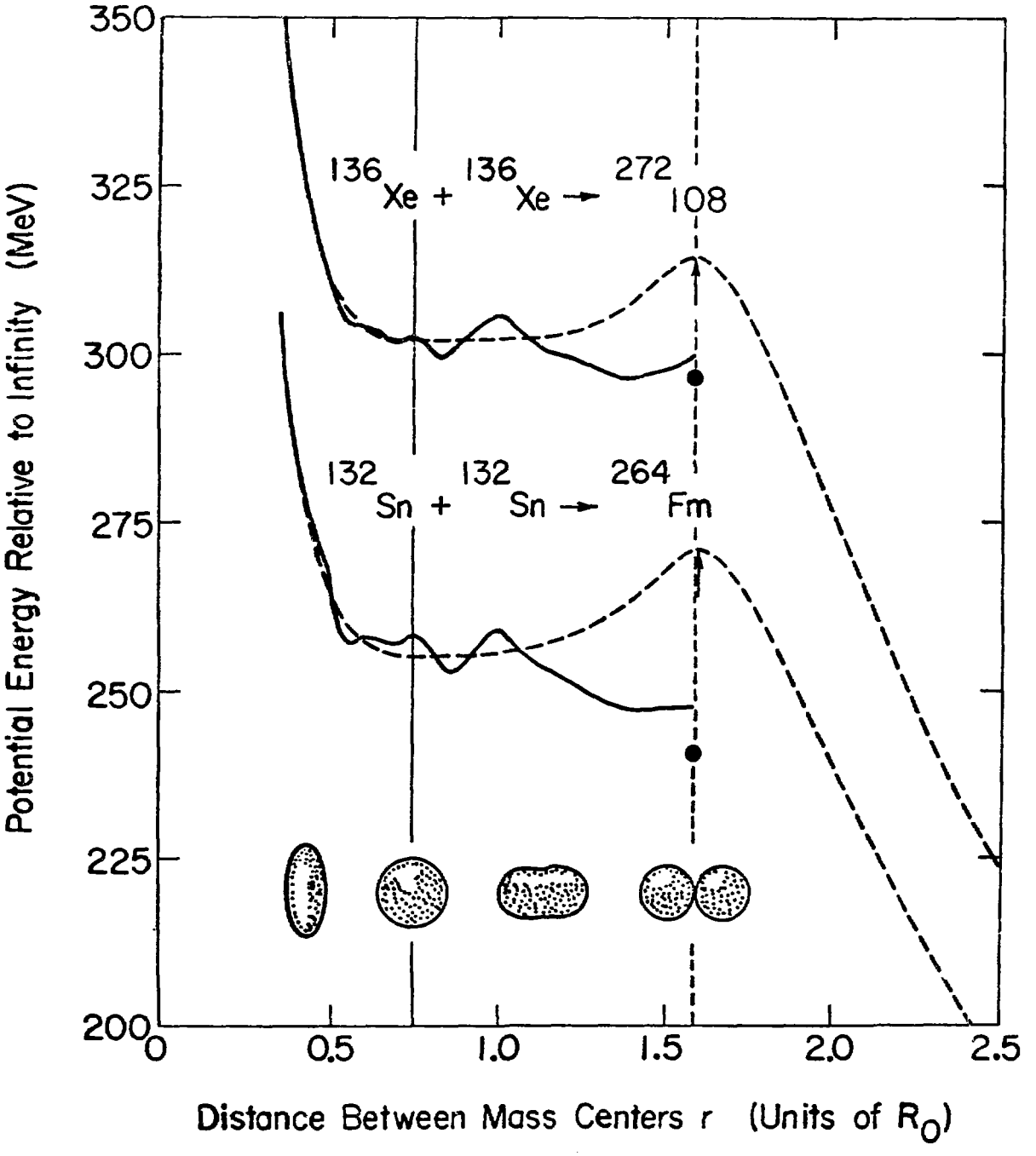
350
325
300
275
250
225
200
0
0.5
1.0
1.5
2.0
2.5
136 Xe + 136 Xe → 272 108
132 Sn + 132 Sn → 264 Fm
Potential Energy Relative to Infinity (MeV)
Distance Between Mass Centers r (Units of R_0)

Figure 3

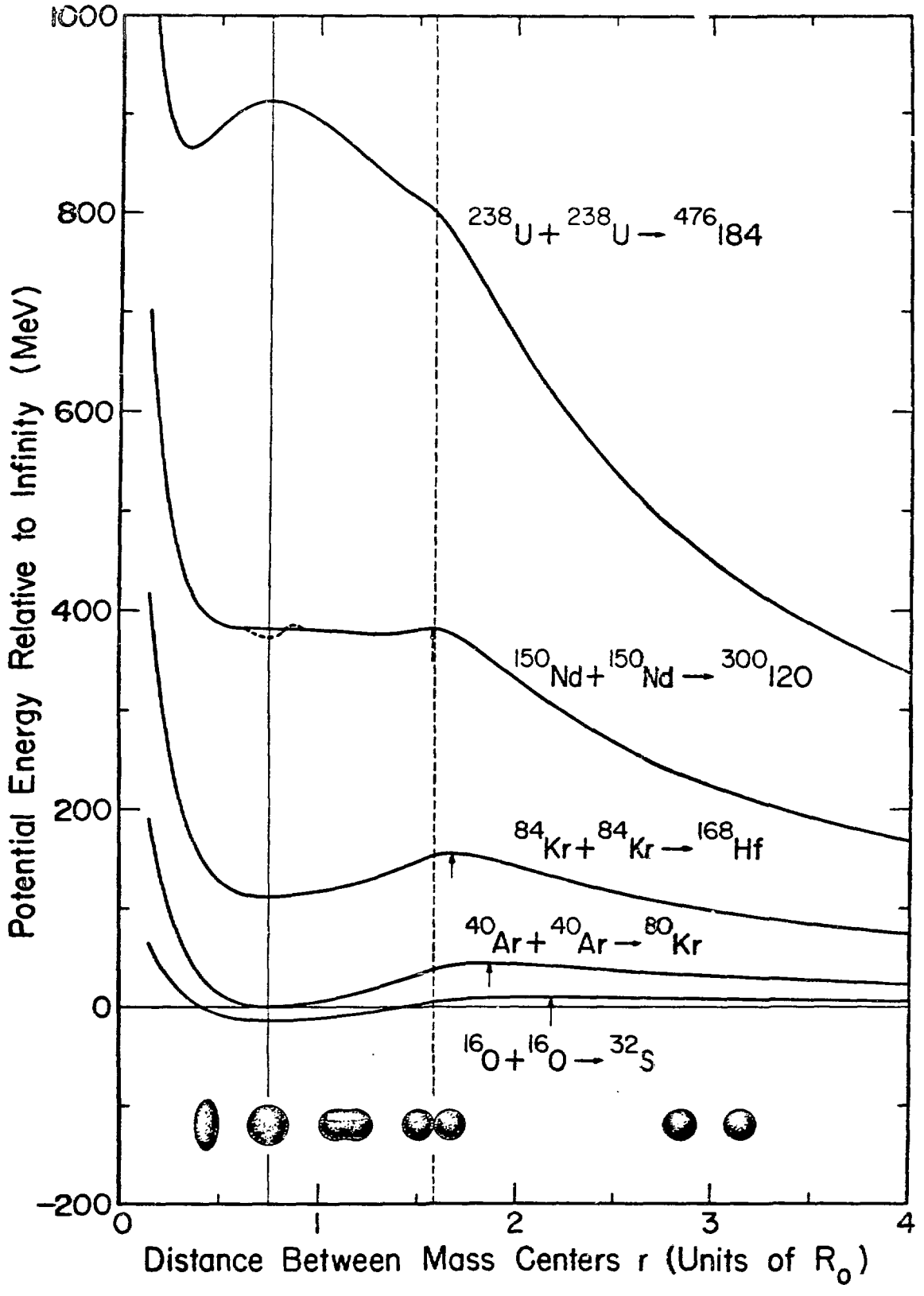
1000
800
600
400
200
0
-200
0
1
2
3
4
Potential Energy Relative to Infinity (MeV)
Distance Between Mass Centers r (Units of R_0)
$^{238}U + ^{238}U \rightarrow ^{476}184$
$^{150}Nd + ^{150}Nd \rightarrow ^{300}120$
$^{84}Kr + ^{84}Kr \rightarrow ^{168}Hf$
$^{40}Ar + ^{40}Ar \rightarrow ^{80}Kr$
$^{16}O + ^{16}O \rightarrow ^{32}S$

Figure 4

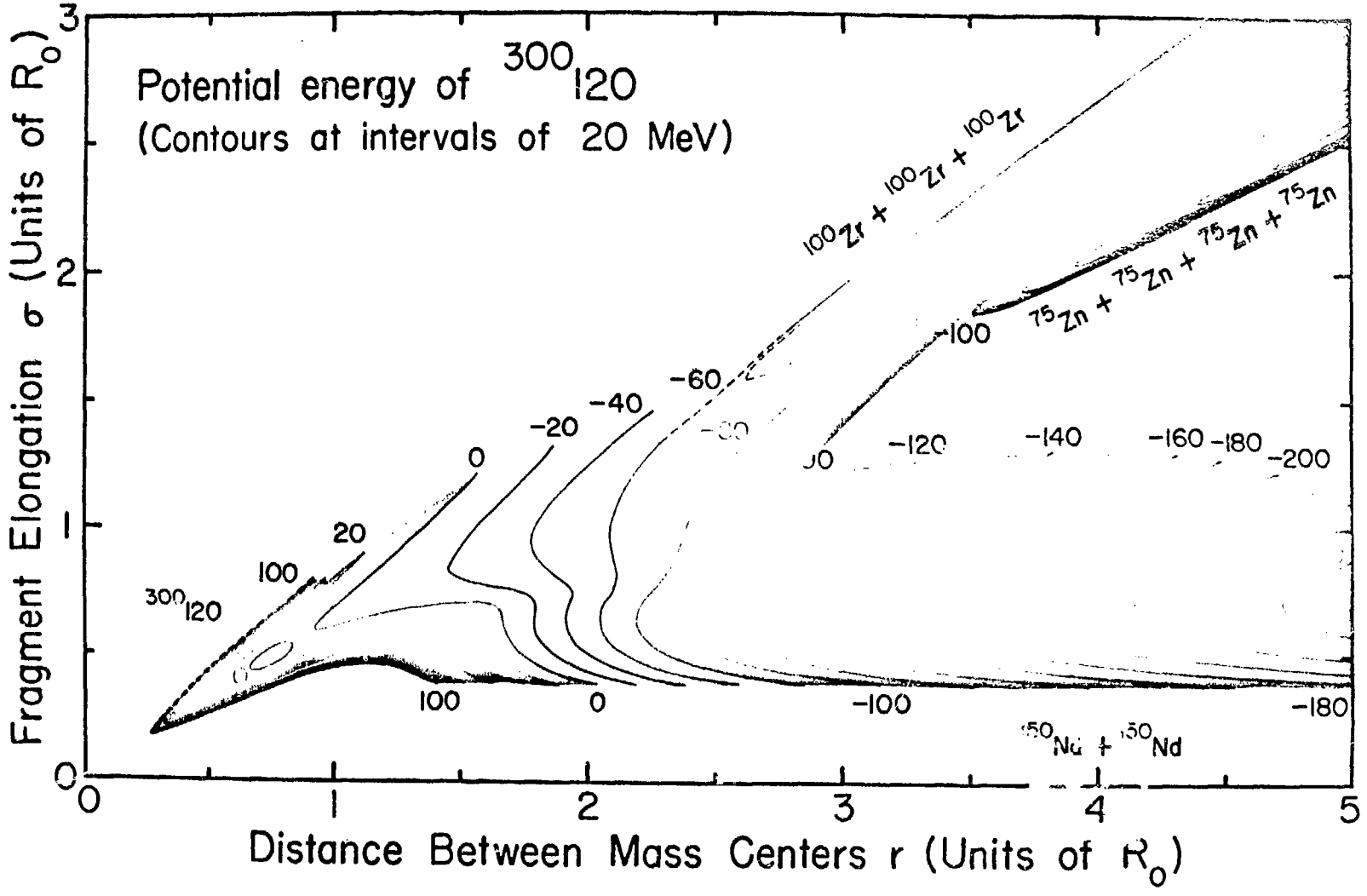
Potential energy of $^{300}120$
(Contours at intervals of 20 MeV)
Fragment Elongation σ (Units of R_0)
Distance Between Mass Centers r (Units of R_0)
$^{100}Zr + ^{100}Zr$
$^{100}Zr + ^{100}Zr + ^{100}Zr$
$^{75}Zn + ^{75}Zn$
$^{75}Zn + ^{75}Zn + ^{75}Zn$
$^{150}Nd + ^{150}Nd$
$^{300}120$
0
20
100
-20
-40
-60
-80
-100
-120
-140
-160
-180
-200

Figure 5

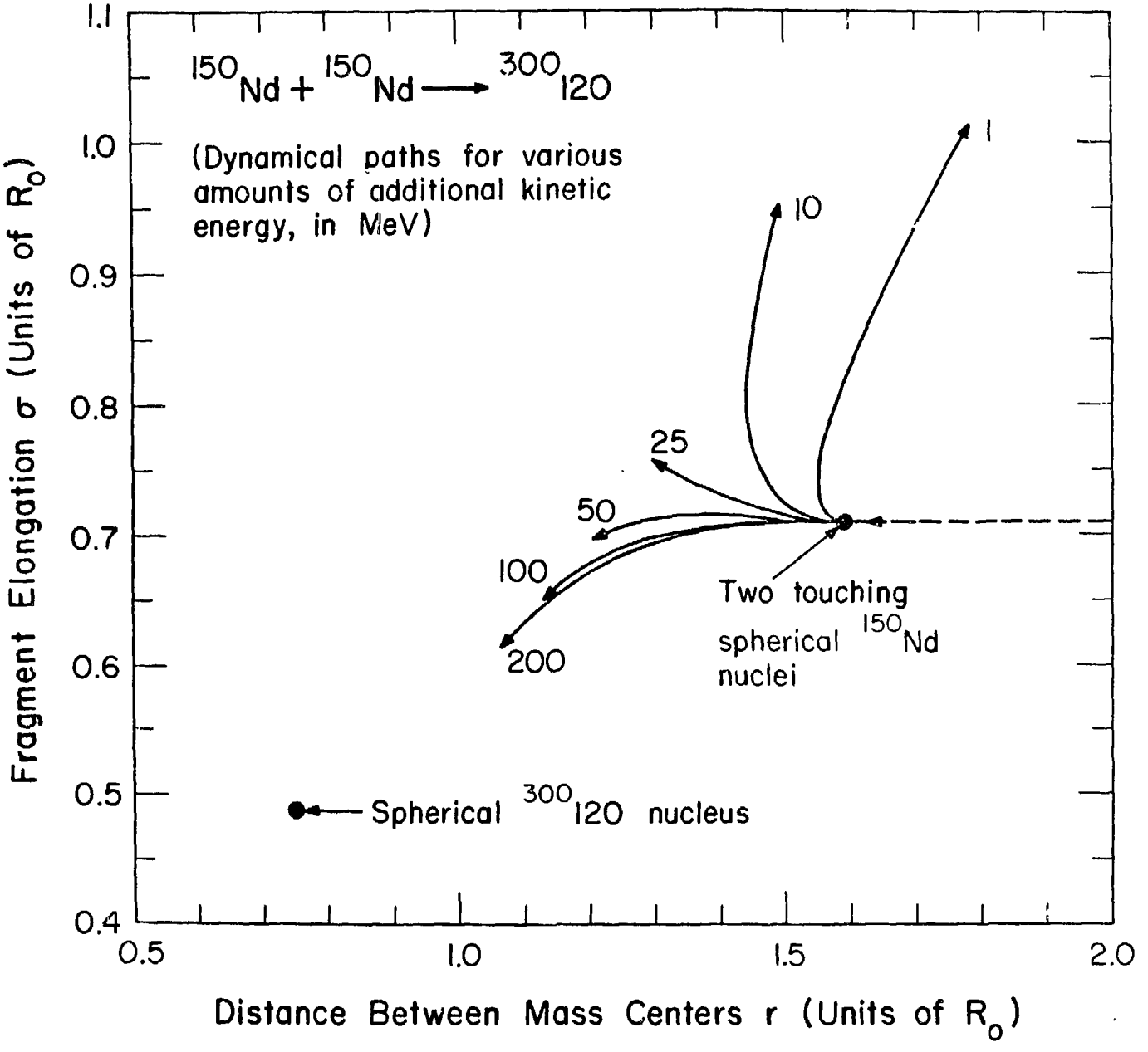
$^{150}Nd + {}^{150}Nd \longrightarrow {}^{300}120$
(Dynamical paths for various amounts of additional kinetic energy, in MeV)
1
10
25
50
100
200
Two touching spherical ^{150}Nd nuclei
Spherical $^{300}120$ nucleus
Fragment Elongation σ (Units of R_o)
Distance Between Mass Centers r (Units of R_o)
1.1
1.0
0.9
0.8
0.7
0.6
0.5
0.4
0.5
1.0
1.5
2.0

Figure 6